Published in "Europhysics Letters 92(4): 47003, 2010"
which should be cited to refer to this work.

Dramatic effective mass reduction driven by a strong potential of competing periodicity

C. Monney[1,2], E. F. Schwier[1], M. G. Garnier[1], C. Battaglia[3], N. Mariotti[1], C. Didiot[1], H. Cercellier[4], J. Marcus[4], H. Berger[5], A. N. Titov[6,7], H. Beck[1] and P. Aebi[1(a)]

[1] *Département de Physique and Fribourg Center for Nanomaterials, Université de Fribourg CH-1700 Fribourg, Switzerland*
[2] *Research Department Synchrotron Radiation and Nanotechnology, Paul Scherrer Institut CH-5232 Villigen PSI, Switzerland*
[3] *EPFL, Institute of Microengineering, Photovoltaics and Thin Film Electronics Laboratory CH-2000 Neuchâtel, Switzerland*
[4] *Institut Néel, CNRS-UJF - BP 166, 38042 Grenoble, France, EU*
[5] *EPFL, Institut de Physique de la Matière Condensée - CH-1015 Lausanne, Switzerland*
[6] *Institute of Metal Physics UrD RAS - Ekaterinburg, 620219, Russia*
[7] *Institute of Metallurgy UrD RAS - Amundsen St. 101, Ekaterinburg, 620016, Russia*

Abstract – We present angle-resolved photoemission experiments on $1T$-$TiSe_2$ at temperatures ranging from 13 K to 288 K. The data evidence a dramatic renormalization of the conduction band below 100 K, whose origin can be related to the new potential responsible for the charge density wave phase at low temperature in this system. The renormalization translates into a substantial effective mass reduction of the dominant charge carriers and this observation is thus in opposition to the common belief that strong interactions produce heavier quasiparticles through an increased effective mass.

Particularly stimulated by the discovery of high-temperature superconductivity, interest in strongly correlated electron systems never ceased to increase in the last decades. Strong correlations in, *e.g.*, heavy-fermion systems involving d- and f-electrons, usually produce weakly dispersive bands in their electronic structure, which give rise to quasiparticles with large effective masses [1]. Coupling of the electronic states to phonon modes [2], as well as the opening of a gap due to a Peierls transition [3], is also known as a possible mechanism for such an effect. In all these examples, strong interactions are commonly considered as responsible for important band renormalizations, leading to increased band effective masses. In the case of $1T$-$TiSe_2$ studied below, it will be shown that the strong potential, responsible for the onset of its charge density wave phase (CDW) at low temperature, results in the opposite effect.

Among the transition metal dichalcogenides, $1T$-$TiSe_2$ is of particular interest [4]. At the critical temperature of $T_c \simeq 200$ K, the system undergoes a phase transition into a CDW phase accompanied by a periodic lattice distortion (PLD) [5]. Around the transition, it displays strongly anomalous transport properties, with a resistivity showing a pronounced peak having its maximum slightly below T_c. The compound has also attracted strong interest since superconductivity has been discovered in the copper-intercalated material, Cu_xTiSe_2 [6], as well as in the pure material under pressure [7]. In the past years, different angle-resolved photoemission spectroscopy (ARPES) studies were carried out on $1T$-$TiSe_2$ [8–11]. They all evidenced two main contributions near the Fermi energy E_F, a Se-4p derived band at the center of the Brillouin zone (BZ) (Γ-point in fig. 1(a)), identified as a valence

(a) E-mail: philipp.aebi@unifr.ch

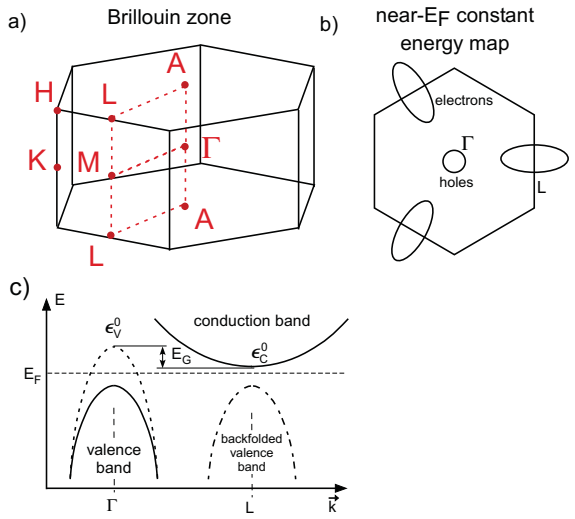

Fig. 1: (Color online) (a) Brillouin zone of $1T$-$TiSe_2$ with its high-symmetry points. (b) Schematized near-E_F constant energy map of $1T$-$TiSe_2$ around Γ and L. (c) At Γ, the gap opening due to the exciton condensation shifts the valence band far below E_F and only the conduction band provides some electronic states near E_F.

band in what follows, and three (symmetry equivalent) Ti-3d derived bands at the border of the BZ (L-point), identified as conduction bands (see fig. 1(b) and (c)).

As the temperature decreases below T_c, an intense backfolded valence band appears at L (dash-dotted line in fig. 1(c)), as direct evidence for the CDW. It is well known that, in the case of a CDW phase, the intensity in the backfolded bands is proportional to the strength of the new potential of competing periodicity [12,13]. Based on the fact that in $1T$-$TiSe_2$ the backfolded valence band displays a high intensity despite the relatively small atomic displacements (~ 0.08 Å) of the PLD [5], we recently gave much support to the exciton condensate phase as the primary origin of the CDW phase in $1T$-$TiSe_2$ [11], which relies on strong electronic interactions, in agreement with the prediction of Wilson *et al.* [14,15].

Originally denominated the "excitonic insulator phase" [16,17], this exotic phase takes the form of a collective phenomenon driven by strong electronic interactions. Its basic ingredients are a valence and a conduction band, having a semimetallic or semiconducting configuration. Then, bound states of holes and electrons, called excitons, can condense at low temperature into a macroscopic state, provided the gap is small and the screening of the Coulomb interaction is weak. For $1T$-$TiSe_2$, this purely electronic effect naturally generates the CDW, opening a gap below the conduction band, which shifts the valence band away from E_F [18]. Since an exciton is a neutral quasiparticle, condensation of such entities removes charge carriers from the system. In fact, this effect already occurs above T_c due to strong electron-hole fluctuations [19].

In this letter, we present temperature-dependent ARPES measurements of $1T$-$TiSe_2$. A dramatic renormalization of the conduction band at low temperature is evidenced. Its origin is qualitatively explained using the exciton condensate phase model and is thus related to the strong potential of competing periodicity developing in the system at low temperature. It results in a strong *reduction* of the electron effective mass.

The photoemission intensity maps presented here were recorded using monochromatized, linearly p-polarized HeIα radiation at 21.2 eV and using an upgraded Scienta SES-200 spectrometer with an overall energy resolution better than 10 meV. A liquid-helium–cooled manipulator having an angular resolution of 0.1° was used, with a temperature stability < 5 K. The $1T$-$TiSe_2$ samples used here are of the same batch than those measured in ref. [19] (having thus a negligible excess of Ti atoms) and were cleaved *in situ*, in a base pressure in the low 10^{-11} mbar, ensuring a high longevity of the sample surface. Photoemission spectra were recorded from 13 K to 288 K. At the end of the measurements, the sample was cooled to 13 K and comparable spectra were recorded again, confirming its stability. Reference spectra of polycrystalline gold evaporated on the same sampleholder were recorded for determining E_F. At the excitation energy of 21.2 eV, at the border of the BZ, initial states close to the L-point are probed (see the BZ depicted in fig. 1(a)). Therefore, to simplify, the notation L will be chosen for these states throughout this article.

For $1T$-$TiSe_2$, below the critical temperature, the main feature in the neighborhood of E_F is the conduction band at L, since the valence band at Γ is shifted to higher binding energies (see fig. 1(c)) [11]. Figure 2 presents photoemission intensity maps of this electron pocket taken at four different temperatures, along the high-symmetry directions AL and LH. Binding energy *vs.* momentum maps highlight the behavior of the dispersion of the conduction band at 288 K, 141 K, 81 K and 13 K in fig. 2(a), (b), (c) and (d), respectively. At 288 K, the conduction band follows a clear wide parabolic dispersion along AL (left panel), with a non-trivial spectral weight distribution that can be understood within the exciton condensate phase model extended to the strong electron-hole fluctuation regime [18]. As the temperature decreases to 141 K (fig. 2(b)), the conduction band gets flatter along AL (left panel). The top of the backfolded valence band is also clearly visible below a binding energy of −0.1 eV. Below 100 K, a dramatic renormalization of the conduction band is visible, as seen in the photoemission intensity maps measured at 81 K and 13 K (fig. 2(c) and (d)). Along AL (left panels), it has no more a simple parabolic shape and divides into different parts. Its branches closer to E_F are getting flatter (hereafter called the heavy part), while it displays a pronounced parabolic dispersion (the light part) in the neighborhood of its minimum.

In order to get the approximate behavior of the quasiparticle dispersion within the temperature-dependent spectral weight distribution close to the Fermi-Dirac cutoff, we perform parabolic fits of the high binding

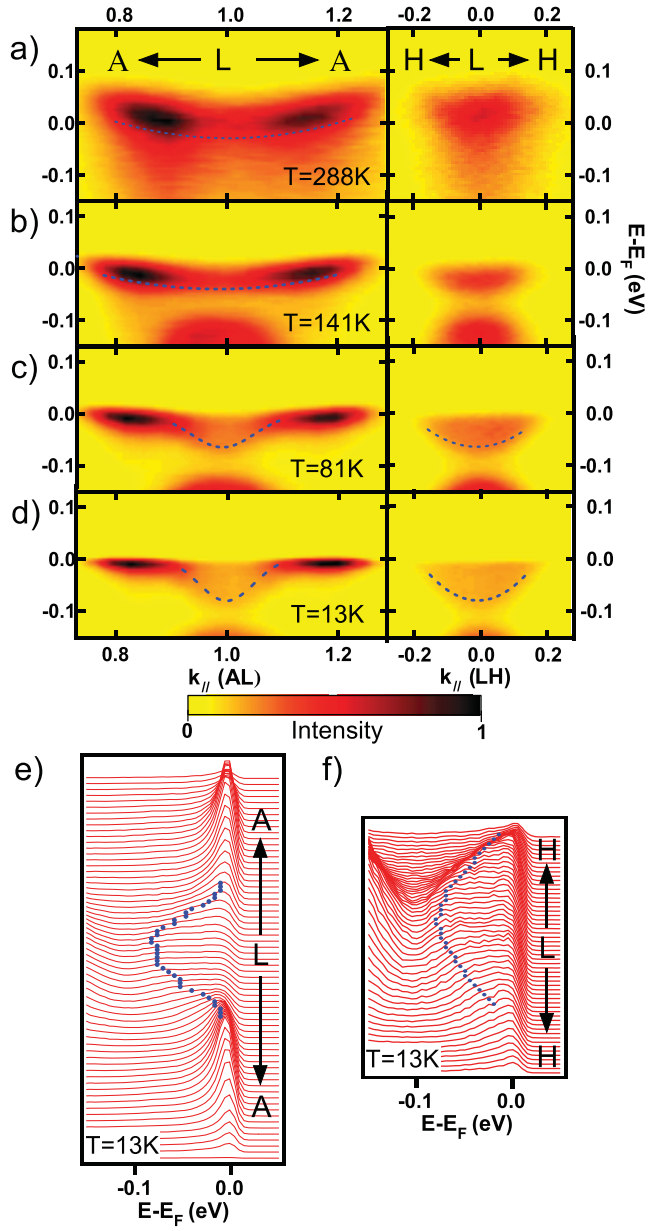

Fig. 2: (Color online) Photoemission intensity maps of the electron pocket around L. (a), (b), (c), (d) Measurements along AL (left panels) and LH (right panels) at 288 K, 141 K, 81 K and 13 K, respectively. (e), (f) Energy distribution curves of the photoemission intensity maps measured at 13 K around L and along AL and LH, respectively. The blue dots indicate the position of the high binding energy edges (see text).

energy edge of the quasiparticle dispersion (defined here as the energy position at which, for each energy distribution curve (EDC), the intensity reaches $\sim 90\%$ of the maximum intensity of the dispersion). This procedure determines the curvature of the dispersions without being strongly affected by intensity variations and by the Fermi-Dirac cutoff varying with temperature[1]. These fits

[1]Indeed, a parabolic band with finite energy width and close to E_F always appears artificially flattened due to the Fermi-Dirac cutoff.

Table 1: Renormalized effective masses of the conduction band (units of bare electron mass) along the long axis (AL) for the light $m_{L,\mathrm{light}}$ and the heavy parts $m_{L,\mathrm{heavy}}$, and along the short axis m_S (LH) of its elliptic Fermi surface, as a function of temperature.

	13 K	81 K	141 K	288 K
$m_{L,\mathrm{heavy}}$	50[(a)]	15[(a)]	6.6(7)	6.2(7)
$m_{L,\mathrm{light}}$	0.4(2)	0.5(2)	6.6(7)	6.2(7)
m_S	0.5(2)	0.8(2)	[(b)]	[(b)]

[(a)] These values have been estimated by a rough parabolic fit.
[(b)] At these temperatures, the procedure to extract m_S becomes inaccurate due to the proximity of the Fermi cutoff.

allow us to estimate the effective mass of the conduction band near its minimum (at L). We show in fig. 2(e) and (f) the high binding energy edges (blue dots) obtained for the photoemission intensity maps measured at 13 K (fig. 2(d)) around L and along AL and LH, respectively, and the corresponding EDCs. Table 1 summarizes the results. This renormalization is so strong that $m_{L,\mathrm{light}}$ is reduced by about a factor 10–15 from 288 K to 13 K. We emphasize here that, in fig. 2, only the temperature has been changed from one measurement to another. This ensures that, in our comparison, the influence of final-state effects or matrix element effects is minimized, since they are expected not to change dramatically from high temperature to low temperature.

The origin of the considerable renormalization of the conduction band can be understood in the framework of the exciton condensate phase model. In this model, the CDW phase is naturally realized, when the order parameter Δ of the exciton condensate phase acquires non-zero values [18]. The electron-hole interaction, responsible for the formation of excitons, couples the three conduction bands to the valence band, so that in the CDW phase, many backfolded bands appear at L, giving rise to a complicated band structure.

Figure 3(a) depicts the situation near E_F for the renormalized dispersions without the spectral weights. Continuous lines represent the main conduction band (blue) c_1 which cohabits with two symmetry equivalent backfolded conduction bands (red) c_2 and c_3, all calculated with an order parameter of $\Delta = 0.1$ eV. The dashed (red) line represents the original ($\Delta = 0$ eV) conduction band, whose minimum is fixed at -55 meV, corresponding to its position measured at 13 K [19]. We see that, for $\Delta = 0.1$ eV and along AL, the main conduction band (blue) c_1 is bent near its minimum (arrows in fig. 3(a)) towards the backfolded conduction band (red) c_2, giving rise to a mass renormalization as observed in our ARPES data. Concerning the renormalization effect, the exact position of the bands with respect to E_F is not important, only their relative position is relevant.

It must be emphasized that this effect does not occur in a model where only *one* conduction band is coupled

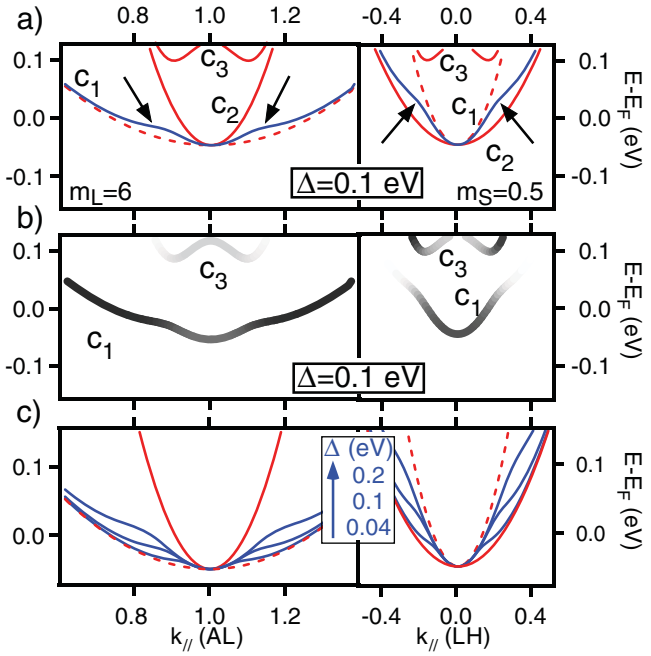

Fig. 3: (Color online) Renormalized band dispersions calculated within the exciton condensate phase model, around L, for $\Delta = 0.1\,\text{eV}$ (a) without the spectral weights and (b) with the spectral weights. The effective masses of the conduction band in the absence of renormalization effects ($\Delta = 0\,\text{eV}$) are fixed to $m_L = 6$ and to $m_S = 0.5$. Dashed lines represent bands calculated with an order parameter $\Delta = 0\,\text{eV}$. The blue line represents the main conduction band c_1. (c) Renormalization of the main conduction band as a function of the order parameter, for $\Delta = 0.04, 0.1, 0.2\,\text{eV}$. The conduction band c_3 is omitted for clarity.

to the valence band [20]. Figure 3(b) depicts the same situation, but now the spectral weights are superimposed on the dispersions in a grayscale coding (black being the maximum spectral weight). In the CDW phase, the spectral weight is transferred from the original band c_1 (dashed red curve in fig. 3(a)), to the backfolded band c_3 (and also to the backfolded valence band which is not shown in fig. 3, as it appears at higher binding energies), but mainly remains on the main conduction band c_1. The conduction band c_2 carries a negligible spectral weight and is thus not visible.

To better understand this effect, we plot in fig. 3(c) the main conduction band c_1 (blue) for different values of the order parameter Δ. It illustrates how strong electron-hole interactions, modelled by the order parameter in our mean-field approach, are responsible for this dramatic renormalization. Along AL (left panel), these calculations clearly show that, while the $\vec{k}$ range over which this band is concerned by the mass renormalization increases with Δ, the reduced effective mass near L (obtained with parabolic fits close enough to its minimum) is always the same, $m_{L,\text{light}} \simeq 1.7$. Simple analytical approximations for the renormalized dispersions performed close to L indicate that this value is in fact related to the non renormalized effective mass m_S. Along LH (right panel), the situation is different, since the main conduction band (blue) always follows its original dispersion (dashed red) near L and undergoes a renormalization (with increased effective mass) only away from L, where mainly empty states (invisible to ARPES) are affected.

In our calculations, the ratio of the effective masses in the absence of renormalization effects, m_L/m_S (*i.e.* without excitonic effects, at $\Delta = 0\,\text{eV}$), plays an essential role in this mass renormalization at lower temperatures. The larger the anisotropy of the electron pocket, the stronger the renormalization effect and thus the lower the effective mass $m_{L,\text{light}}$. In fig. 3, we used a ratio of $m_L/m_S = 12$, which is close to what is observed here ($m_L/m_S \simeq$ 10–15), and is already high enough to produce a substantial renormalization at lower temperatures.

These results are in good agreement with our experimental observations, except for the calculated value of $m_{L,\text{light}} \simeq 1.7$ which underestimates the strength of the renormalization inferred from our ARPES data. We emphasize here that the exciton condensate phase model, which gives rise to the observed CDW, relies only on electronic degrees of freedom [11,18]. However, the PLD, which is concomitant with the CDW and which is not considered in our model, may enhance the anisotropy of the electron pocket, thus giving rise to a larger renormalization and reconciling the theoretical value of $m_{L,\text{light}}$ with the experimental one.

Looking at the data of fig. 2, one may argue that the electronic structure at low temperature (at L) consists of two bands, a "light" one (close to L) and a "heavy" one (giving rise to the high-intensity parts further from L), so that the heavy one is present at all temperatures and that it is progressively cut by the Fermi-Dirac distribution, giving the belief that its effective mass increases as the temperature decreases. The light band would then appear at low temperature as a backfolded band due to the CDW phase. However, such an alternative scenario is unreasonable for the following reasons. First, there is no trace of this backfolded light band at L at 141 K (see fig. 2(b)), where the CDW phase is already present. Second, according to the symmetry of the lattice and the equivalence of the conduction bands, the different conduction bands close to E_F (c_1, c_2) must be degenerate at their minimum at L in the CDW phase (see fig. 3) [18].

The substantial renormalization of the conduction band unveiled in this work must have an influence on the resistivity of $1T$-$TiSe_2$, which displays two opposite behaviors at different temperature regimes [5]. As the temperature decreases below 300 K, the resistivity quickly increases, reaching a maximum at about 180 K. In the framework of the exciton condensate phase, a gap, already present above T_c due to electron-hole fluctuations, shifts the valence band away from E_F and spectral weight is removed from the conduction band at the same time [18,19]. Therefore, the number of charge carriers near E_F available for

transport is reduced and the resistivity increases. Below $\sim 180\,\mathrm{K}$, the resistivity of $1T$-$TiSe_2$ decreases again to values similar to those measured at room temperature. The dramatic renormalization evidenced in this work gives an indication towards the understanding of this decrease: in the framework of the Drude formula, a reduced effective mass leads to a reduced resistivity. However, more complicated calculations using, *e.g.*, the Boltzmann equation in the framework of the exciton condensate phase should be carried out to get a full understanding of the resistivity of $1T$-$TiSe_2$. Furthermore, the complete geometry of the Fermi surface of $1T$-$TiSe_2$ (with electron pockets having different orientations) must be taken into account.

In conclusion, we have evidenced a dramatic renormalization in the band structure of $1T$-$TiSe_2$ at $T < 100\,\mathrm{K}$. The effective mass decreases by a factor 10–15 with respect to its room temperature value. In the framework of the exciton condensate phase model, inferring strong electron-electron interactions, we are able to reproduce qualitatively this effect. Therefore, in opposition to the common belief, strong electronic interactions here give rise to a substantial effective mass *reduction* of the dominant charge carriers.

* * *

We thank F. Baumberger and L. Forrò for valuable discussions. We wish to acknowledge support from our mechanical workshop and electronic engineering team. This project was supported by the Fonds National Suisse pour la Recherche Scientifique through Div. II and the Swiss National Center of Competence in Research MaNEP.

REFERENCES

[1] Fujimori A. and Tokura Y., *Rev. Mod. Phys.*, **70** (1998) 1039.
[2] Hengsberger M., Purdie D., Segovia P., Garnier M. and Baer Y., *Phys. Rev. Lett.*, **83** (1999) 592.
[3] Peierls R. E., *Quantum Theory of Solids* (Oxford University Press) 1955.
[4] Clerc F., Battaglia C., Cercellier H., Monney C., Berger H., Despont L., Garnier M. G. and Aebi P., *J. Phys.: Condens. Matter*, **19** (2007) 355002.
[5] Di Salvo F. J., Moncton D. E. and Waszczak J. V., *Phys. Rev. B*, **14** (1976) 4321.
[6] Morosan E., Zandbergen H. W., Dennis B. S., Bos J. W. G., Onose Y., Klimczuk T., Ramirez A. P., Ong N. P. and Cava R. J., *Nat. Phys.*, **2** (2006) 544.
[7] Kusmartseva A. F., Sipos B., Berger H., Forro L. and Tutis E., *Phys. Rev. Lett.*, **103** (2009) 236401.
[8] Pillo T., Hayoz J., Berger H., Lvy F., Schlapbach L. and Aebi P., *Phys. Rev. B*, **61** (2000) 16213.
[9] Kidd T. E., Miller T., Chou M. Y. and Chiang T.-C., *Phys. Rev. Lett.*, **88** (2002) 226402.
[10] Rossnagel K., Kipp L. and Skobowski M., *Phys. Rev. B*, **65** (2002) 235101.
[11] Cercellier H., Monney C., Clerc F., Battaglia C., Despont L., Garnier M. G., Beck H., Aebi P., Patthey L., Berger H. and Forrò L., *Phys. Rev. Lett.*, **99** (2007) 146403.
[12] Voit J., Perfetti L., Zwick F., Berger H., Margaritondo G., Grüner G., Höchst H. and Grioni M., *Science*, **290** (2000) 501.
[13] Clerc F., Battaglia C., Bovet M., Despont L., Monney C., Cercellier H., Garnier M. G., Aebi P., Berger H. and Forrò L., *Phys. Rev. B*, **74** (2006) 155114.
[14] Wilson J. A. and Mahajan S., *Commun. Phys.*, **2** (1977) 23.
[15] Wilson J. A., *Phys. Status Solidi B*, **86** (1978) 11.
[16] Keldysh L. V. and Kopaev Y. V., *Fiz. Tverd. Tela (Leningrad)*, **6** (1965) 2791; *Sov. Phys. Solid State*, **6** (1965) 2219.
[17] Jérome D., Rice T. M. and Kohn W., *Phys. Rev.*, **158** (1967) 462.
[18] Monney C., Cercellier H., Clerc F., Battaglia C., Schwier E. F., Didiot C., Garnier M. G., Beck H., Aebi P., Berger H., Forrò L. and Patthey L., *Phys. Rev. B*, **79** (2009) 045116.
[19] Monney C., Schwier E. F., Garnier M. G., Mariotti N., Didiot C., Beck H., Aebi P., Cercellier H., Marcus J., Battaglia C., Berger H. and Titov A. N., *Phys. Rev. B*, **81** (2010) 155104.
[20] Halperin B. I. and Rice T. M., *Solid State Phys.*, **21** (1968) 115.